Comparative Medicine
Copyright 2020
by the American Association for Laboratory Animal Science

Vol 70, No 3
June 2020
Pages 258–265

Original Research

Assessment of Semi-automated Computed Tomographic Measures of Segmental Perfusion Defects in a Swine Model (*Sus scrofa*) of Intermediate Coronary Lesions

Bryan C Ramsey,[1] Amy E Field,[2] Dustin M Thomas,[1] Christopher A Pickett,[1] Alisa J Leon,[2] and Bernard J Rubal,[1,*]

Computed tomographic myocardial perfusion (CTP) imaging is a tool that shows promise in emergent settings for defining the hemodynamic significance of coronary artery disease. In this study, we examined the accuracy with which the transmural perfusion ratio (TPR) derived through semiautomated CTP analysis reflected segmental perfusion defects associated with intermediate coronary artery lesions in swine. Lesions (diameter stenosis, 65% ± 11%) of the left anterior descending coronary artery (LAD) were created in 10 anesthetized female swine (weight, 47.5 ± 1.9 kg) by using a pneumatic occlusion device implanted on the LAD. Occluder inflation pressures were adjusted to maintain fractional flow reserve (FFR, 74.3 ± 1.7) during adenosine infusion (140ug/kg/min). Static CTP imaging using a stress-rest protocol and segmental TPR derived from semiautomated CT perfusion software was compared with microsphere-derived TPR (mTPR) by using a 16-segment model and polar mapping. Intermediate LAD stenosis was verified through multiplanar coronary CT angiography. Receiver operating characteristic analysis identified an optimal threshold for segmental perfusion defects for intermediate lesions (TPR threshold, ≤0.80); however, the area under the receiver operating characteristic curve was 0.58, and the overall accuracy was 63%. At this threshold, the sensitivity and specificity were 65% and 61%, and the positive and negative predictive values were 61% and 65%, respectively. Although CTP–TPR illustrated segmental perfusion defects with intermediate lesions, the disparity between CTP–TPR and mTPR measures of segmental perfusion suggests that further advances in analysis software may be necessary to improve the localization of segmental defects for intermediated lesions.

Abbreviations: CCTA, cardiac CT angiography; CTP, CT myocardial perfusion; CTP–TPR, CTP-derived TPR; FFR, fractional flow reserve; LAD, left anterior descending; LV, left ventricle; mTPR, microsphere-derived TPR; SPECT, single-photon emission CT; TPR, transmural perfusion ratio

DOI: 10.30802/AALAS-CM-19-000104

Cardiac CT angiography (CCTA) has high sensitivity for ruling out obstructive coronary artery disease.[16,18,21] CCTA allows for the visualization of epicardial vessels by using intravenous injection of contrast media and is without complications associated with invasive cardiac catheterization procedures. This method of coronary artery visualization is arguably the best first-line test to exclude obstructive coronary artery lesions in patients with low to intermediate risk of chest pain and who lack known coronary artery disease.[12,24,25] However, a limitation of CCTA is the accurate diagnosis of hemodynamically significant lesions in the setting of a 50% to 69% epicardial stenosis (i.e., intermediate lesions). Patients with intermediate lesions present a clinical conundrum with ischemic symptoms often presenting only during stress. Roughly 50% of these patients will not have ischemia and thus may not benefit from revascularization procedures.[2,4] Recent advances in CT technology and image processing suggest that contrast-enhanced CT myocardial perfusion (CTP) imaging has potential for not only defining coronary artery anatomy but also identifying the hemodynamic significance of coronary lesions in a single test procedure. Various CTP indices have been proposed to quantify ischemic burden.

In clinical trials, CTP indices of myocardial perfusion were compared with single-photon emission CT (SPECT), MRI, and invasive measures of fractional flow reserve (FFR).[1,3,13-15,17,29] When compared with SPECT stress perfusion studies, CTP indices derived during pharmacologic stress are reported to have a sensitivity ranging from 86% to 96%, specificity of 65% to 100%, and a positive predictive value of 78% to 100% for detecting perfusion defects.[10,11,14] Given that the endocardium is more sensitive to ischemia than the epicardium, one group introduced a semiautomated CTP method for assessing the myocardial ischemia using the transmural perfusion ratio (TPR).[13] In those and other studies, myocardial segments with TPR of less than 0.99 were considered ischemic.[10,13,14,22] The authors reported that TPR improved the specificity of CCTA for accurately identifying obstructive stenosis. However, the patient populations in these

Received: 24 Oct 2019. Revision requested: 09 Dec 2019. Accepted: 20 Dec 2019.
[1]Cardiology Service, Brooke Army Medical Center, and [2]US Army Institute of Surgical Research, Fort Sam Houston, Texas
[*]Corresponding author. Email: bernard.j.rubal.civ@mail.mil

studies had a wide spectrum of coronary disease. The incremental benefit in specificity for patients with intermediate stenosis is not well established. In present study, we examine the accuracy CTP measures of TPR in swine with intermediate LAD lesions established by the titration of an occlusion device during adenosine infusion compared with microsphere-based measures of segmental blood flow (mTPR).

Materials and Methods

Figure 1 provides a schema of the procedures and protocol for this experiment. The animal protocol was reviewed and approved by the IACUC at the US Army Institute of Surgical Research (protocol no. A17-01). This study has been conducted in compliance with the Animal Welfare Act,[30] the implementing Animal Welfare Regulations,[30] and the principles of the Guide for the Care and Use of Laboratory Animals.[20]

Ten female Yorkshire swine (*Sus scrofa*; weight, 47.5 ± 1.9 kg) were sedated by using intramuscular injection of tiletamine–zolazepam (4 to 5 mg/kg; Fort Dodge Animal Health, Fort Dodge, IA). The animals were anesthetized by using 4% to 5% isoflurane (Baxter, Deerfield, Ill.) and 100% oxygen by face mask. After endotracheal intubation, they were maintained on 2% to 3% isoflurane with 100% oxygen. Vascular access was established for catheter placement in the femoral arteries, left carotid artery, and jugular vein. Left lateral thoracotomy was performed at the fourth intercostal space, and the heart was exposed via a pericardial cradle. A 2.0- or 3.0-mm vascular occluder (Docxs Biomedical, Ukiah, CA) was placed on the proximal to mid left anterior descending coronary artery (LAD) distal to the first septal perforator, to avoid obstruction of septal and diagonal branches. A custom left atrial catheter (inner diameter, 0.062 in.; silastic tubing, Dow Corning) was then directly placed and secured by using a purse-string suture. The pericardial cradle was released, the left atrial catheter and actuating tubing for the occluder were exteriorized, and the chest was closed. After chest closure, animals were transitioned to continuous-rate infusion of total intravenous anesthesia comprised of ketamine HCl (20 to 30 mg/kg/h; Boehringer Ingelheim Vetmedica, Duluth, GA), midazolam HCL (1.0 to 1.5 mg/kg/h; West-Ward Pharmaceuticals, Eatontown, NJ,) and propofol (100 µg/kg; Sargent Pharmaceuticals, Schaumburg, IL) and were maintained under a surgical plane of anesthesia, with mechanically ventilation for arterial pO_2 saturation of greater than 95% and pCO_2 at 40 ± 4 mm Hg, for the remainder of the experiment. ECG, heart rate, arterial blood pressure, oxygen saturation, and expired pCO_2 were continuously monitored.

Retrograde cardiac catheterization was performed via the right femoral artery under fluoroscopic guidance for the placement of a 2-French high-fidelity catheter (model 814, Mikro-Tip, Millar Instruments, Houston, TX) in the LAD distal to the LAD occluder. This goal was accomplished by using a 6-French, Amplatz Left (AL.75) guide catheter (Runaway, Boston Scientific, Marlborough, MA), 5.5-French Guideliner (Vascular Solutions, Maple Grove, MIN), and 0.014-in. coronary wire as needed. Arterial pressures were simultaneously obtained both from the arterial sheath and a 6-French high-fidelity catheter (Mikro-Tip, Millar Instruments) placed in the central aorta. Both phasic and mean pressures were recorded from each recording site. Fractional flow reserve (FFR) was continuously computed and displayed in real-time as:

$$\text{FFR} = \frac{\text{mean} \times P_d}{\text{mean} \times P_a}$$

Mean P_d is the mean coronary pressure distal to the occluder, and mean P_a is mean aortic pressure. Hyperemia was induced by the intravenous infusion of adenosine (140 µg/kg/min; Sigma-Aldrich, St Louis, MO). After hemodynamic stabilization during hyperemia, an intermediate LAD lesion (FFR, approximately 75% [74.3% ± 1.7%]) was achieved by the controlled inflation of the LAD occluder (Encore Inflator, Boston Scientific, Marlborough, MA). The occlusion was maintained but the adenosine infusion was suspended while the animal transported for CT imaging.

CT perfusion protocol. Hyperemia was again induced by adenosine infusion (140 µg/Kg/min) prior to CT myocardial perfusion imaging. Static CT cardiac tissue perfusion imaging using a stress-rest protocol[5,6] with retrospective, ECG-gated acquisition was performed (Aquilion Prime, Cannon Medical Systems, Irvine, CA). With this CT perfusion protocol, myocardial perfusion is first assessed during vasodilation with adenosine then following a period of recovery the resting state images are obtained.[5,6] Arterial blood pressure and ECG were continuously monitored.

After hemodynamic stabilization and scout imaging, a power injector (MEDRAD Stellant, Bayer HealthCare, Whippany, NJ) was used for triphasic infusion of intravenous-contrast iopamidol (Isovue-370, Bracco Diagnostics, Monroe Township, NJ) and saline (contrast, 4.0 mL/s for 44 mL; mix, 4.0 mL/s for 22 mL; saline, 4.0 mL/s for 50 mL). All images were acquired at held expiration. CT image acquisition was initiated by using bolus tracking (Sure Start, Cannon-Toshiba, Tustin, CA), with the region of interest located on the descending aorta at or just below the level of the carina and a threshold for acquisition set as +180 HU. Retrospective ECG-gated scans were acquired at 120 kV and 400 mA. Images were reconstructed at a slice thickness of 0.5 mm between 0% and 90% of the R-R interval.

In addition, grayscale CT perfusion images were interpreted visually by an experienced cardiologist (DT), who was blind to quantitative stenosis results. The postprocessing settings used for visual interpretation of myocardial perfusion were 5-mm slabs with Hounsfield unit averaging and window width and level of 300 and 100 HU, respectively. Left ventricular (LV) wall-motion assessments were made by using the workstation cine function and formatted in traditional transthoracic echocardiography views. Semiautomated measures of TPR were assessed based on a 16-segment perfusion model (apex excluded, with slices modified for 1-cm slice thickness) previously reported, with manual correction of the epicardial and endocardial borders when applicable.[13,14]

Myocardial blood flow. Myocardial blood flow was obtained from microsphere measurements immediately after CT image acquisition while adenosine infusion was maintained. A dose of 8.0×10^6 microspheres (15-µm microspheres, BioPAL, Wellesley Hills, MA) was delivered in 7 mL of normal saline bolus via the left atrium, followed immediately by a 7-mL flush of normal saline. A reference arterial blood sample was withdrawn from the left femoral artery sheath at a rate of 3 mL/min for 3.5 min, beginning 30 s prior to microsphere injection. Microsphere measurement of myocardial tissue perfusion was previously validated.[27] Adenosine infusion was then terminated, and 20 min was allowed for recovery from hyperemia. Resting CT myocardial perfusion imaging was then performed, followed by a second injection of microspheres with a different stable isotope label.

At the completion of CT imaging and microsphere injections, total occlusion of the LAD was achieved by inflation of the occluder. A 3% solution of Evan blue dye (Sigma-Aldrich)

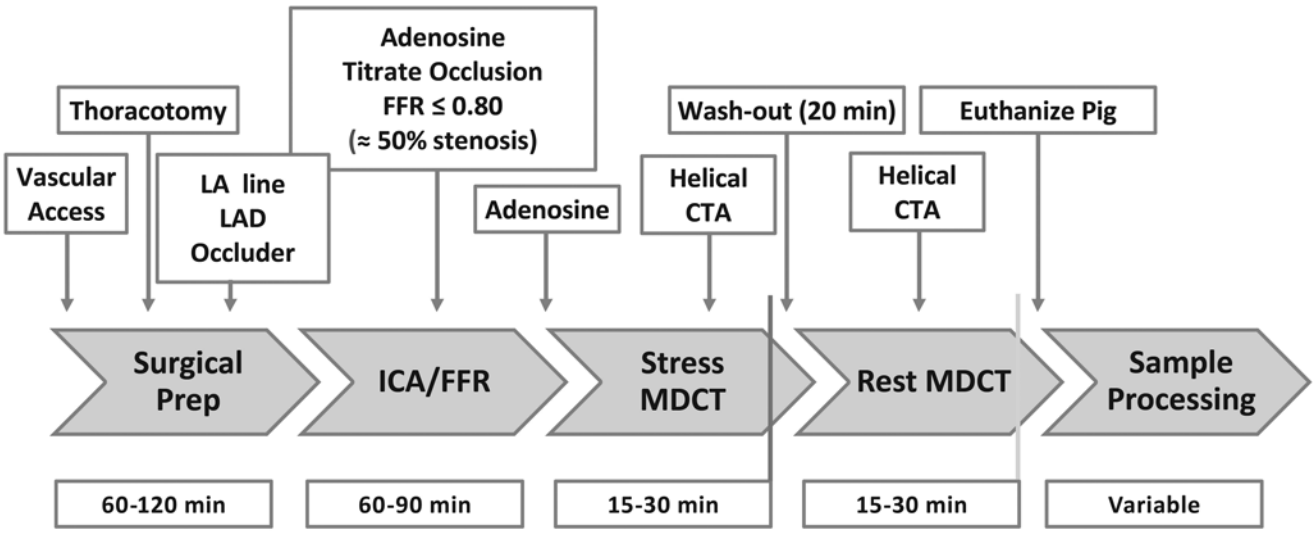

Figure 1. Schema of the protocol, from animal preparation through tissue sample processing. CTA, computed tomography angiography; FFR, fractional flow reserve; ICA, intracoronary angiography; MDCT, multidetector computed tomography; LA line, left atrial fluid line; and LAD, left anterior descending coronary artery, occluder. The vertical green and gold lines indicate microsphere injections.

was injected into the LV cavity (n = 8) or into the LAD distal to the occluder post mortem (n = 2). Animals were euthanized (Fatal Plus, Vortech Pharmaceuticals, Dearborn, MI) and the heart extracted. The LV was weighed (wet weight) after removal of the left and right atria, right ventricle, pulmonary artery, and aorta. The LV was then cooled for 24 h at 10 °C. The heart was then cooled at –15 °C for 30 min and cut into uniform-thickness (10 ± 1.0 mm) short-axis slices (model 61-0901, Weston, Strongsville, OH). These short-axis slices were photographed for correlation with CT perfusion imaging. The papillary muscles and valvular apparatus were removed, and short-axis segments were indexed in accordance with the 16-segment model[13] modified to incorporate the greater spatial resolution of the anatomic slices our study. In the present study, myocardial blood flow was assessed from the short-axis slice beginning at the level of the occluder to the apical region (the apical cap was not included). The basal slice above the occluder was excluded also. Three short-axis slices (approximately 1-cm thick; 2 mid-cavity and one apical) were analyzed from each animal. The short-axis slices were then cut into perfusion territories for the LAD, left circumflex, and right circumflex arteries by using the anatomic course of the LAD to identify free-wall and septal segments. This process yielded 6 segments from the LAD territory per animal (total of 60 samples) and 10 nonLAD segments (total of 100 non-LAD samples). These segments were then subdivided into endocardial (n = 160) and epicardial (n = 160) sections by using mid-myocardial dissection. The wet weight (mean ± 1 SD) of the epicardial samples was 1.78 ± 0.61 g, the endocardial sample weight was 1.51± 0.62 g, and the overall weight of myocardial samples was 1.65 ± 0.63 g (n = 320 segments). The tissue samples were dehydrated (model 75-0301, Weston) and sent to a core laboratory (BioPAL, Worcester, MA) for analysis by neutron activation.

Data analysis. Both rest and stress CT perfusion images were reviewed by using 3D CT workstation software (Vitrea version 6.7, Vital Images, Minnetonka, MN). Qualitatively, CTP was assessed by a single reader using thin-slab reconstructions (5-mm slices), average and minimal intensity projections at a window width of 200 HU, and a window level of 100 HU. The TPR was derived using semiautomated, proprietary CTP software (Vitrea version 6.7, Vital Images) and previously published methods[13] as

$$\text{CTP} - \text{TPR} = \frac{\text{subendocardial (HU)}}{\text{mean epicardial (HU)}}.$$

Absolute myocardial blood flow (mL/min/g) for subendocardial and epicardial regions was derived by using published microsphere methods[27] as

$$\text{Tissue Blood flow} = \frac{\text{reference blood volume}}{\text{withdrawal time}} \times \frac{\text{activity tissue}}{\text{activity blood}}$$

and

$$\text{mTPR} = \frac{\text{subendocardial blood flow } / \ g}{\text{epicardial blood flow } / \ g}.$$

Continuous variables are presented as mean ± 1 SD, and nominal data are expressed as percent of total. ANOVA was used to assess difference between in blood flow between stress and rest, transmural flow and blood flow between perfusion territories, and segmental perfusion difference in TPR derived by using microspheres and CT. Posthoc tests were used for multiple-group comparisons. Differences in nominal data were assessed through contingency testing or z-tests. P values less than 0.05 were considered significant. Bland–Altman plots and the Cohen κ statistic were used to assess agreement between mTPR and CTP–TPR values. The optimal threshold for CTP–TPR compared with mTPR was assessed by examining sensitivity and specificity curves over the observed range of the TPR values. The receiver operating characteristic curve including the AUC is presented for CTP–TPR, with mTPR as the standard. Statistical

analyses were performed by using commercially available software (SPSS version 22.0, IBM, Armonk, NY, and SigmaPlot, version 12, Systat Software, San Jose, CA).

Results

Intermediate lesion severity. In this study, intermediate coronary lesions were induced in 10 animals by the partial occlusion (diameter stenosis, 65.1% ± 11.0%) of the LAD distal to the first septal perforator during adenosine infusion (FFR, 74.3% ± 1.7%). The mean arterial pressure was lower ($P < 0.001$) with adenosine (50.4 ± 8.2 mm Hg) compared with rest (81.7 ± 9.9 mm Hg). The average heart rate was 81.8 ± 14.0 bpm during adenosine infusion compared with 74.9 ± 11.7 bpm ($P = 0.086$) at rest. Figure 2 illustrates an example of a 3D reconstructed cardiac image with a stress color CTP overlay, multiplanar reconstructions of stress or rest CCTA of the LAD artery, short-axis stress or rest CTP images at the mid-cavity level, and color polar maps of the stress or rest CTP–TPR for a representative animal. In this example, diameter stenosis during adenosine was 61%, and the ischemic territories are indicated with arrows in planar images and as red and black territories on polar maps. The location of the occluder is represented by the letter O.

Myocardial perfusion and TPR. Table 1 compares epicardial and endocardial blood flows (mL/min/g) derived from microsphere measurements and segmental rest and stress TPR. No difference was found between endocardial and epicardial blood flows within the LAD and nonLAD segments at rest. Overall ($n = 160$ segments), the average increase in blood flow with adenosine was 89.6% ± 1.7% in the epicardium compared with 48.0% ± 1.6% within the endocardium ($P < 0.001$). Although significant decreases in mTPR were noted with adenosine, little change was noted in mean CTP–TPR values.

Agreement between mTPR and CTP–TPR. Figure 3 presents the Bland–Altman limits of agreement (mean Δ ± 95% CI = –0.047 ± 0.292) between mTPR and CTP–TPR. The wide variability in the differences indicates poor agreement between TPR measures for intermediate LAD lesions. No significant offset bias ($P = 0.217$) was observed; however, regression of the differences to the mean suggests that a proportion error between mTPR and CTP–TPR was present over the mean measurement range ($R^2 = 0.313$, $P < 0.001$).

Sensitivity and specificity. Figure 4 illustrates the discriminatory value of CTP–TPR for detecting segmental perfusion defects associated with intermediate LAD lesions. Panel A shows an optimal tradeoff between sensitivity and specificity (dashed line) at a TPR threshold of 0.80. At this threshold, there was no difference ($P = 0.855$) in the number of ischemic LAD segments identified by using mTPR (29 of 60, 48.3%) or CTP–TPR (31 of 60, 51.7%). Sensitivity and specificity were 65.5% and 61.3%, and positive and negative predictive values were 61.3% and 65.5%, respectively. The overall accuracy of CTP–TPR was 63.3%, with only fair agreement between CTP–TPR and microsphere TPR when observations were adjusted for chance ($\kappa = 0.267$, $P = 0.038$). Table 2 summarizes the sensitivity, specificity, and predictive values for commonly reported CTP–TPR thresholds and for values that define the color coding on polar maps. The receiver operating characteristic curve (panel B) suggests that the CTP–TPR associated with intermediate lesions has a poor discrimination value for identifying ischemic segments (AUC = 0.581).

CTP–TPR compared with visibly apparent defects and wall-motion abnormalities. In our study, 70% of the animals (7 of 10) had wall-motion abnormalities affecting one or more segments within the LAD distribution during adenosine infusion, and perfusion defects were apparent visually in 60% of the animals (6 of 10). Although all animals with visible CT perfusion defects had at least one LAD segment with CTP–TPR of 0.8 or less, 3 animals without visible perfusion defects also had segments in which CTP–TPR was 0.8 or less. In addition, 6 of the 7 animals with wall-motion abnormalities had at least one hypoperfused segment, and 3 animals without wall-motion abnormalities had CTP–TPR of 0.80 or less. Therefore, although best agreement in LAD segmental perfusion was noted between mTPR and CTP–TPR at a threshold of 0.80, poor overall agreement was noted between CTP–TPR and both visible perfusion ($\kappa = 0.286$, $P = 0.197$) and wall-motion ($\kappa = 0.176$, $P = 0.490$) defects.

Discussion

Although the benefits of CT angiography for identifying the anatomic location of epicardial lesions are well established, the physiologic significance of epicardial lesions is poorly defined by angiography alone.[7,19,28] This situation is particularly true for intermediate lesions.[28] The clinical challenge with these lesions is to determine whether the patient will benefit from a revascularization procedure. Typically, these patients have sufficient coronary perfusion in the resting state to prevent ischemia. However, under stress, when myocardial perfusion demands increase, ischemic regions develop in myocardial segments downstream from the lesion. With the advances in CT imaging over the past decade, novel approaches have evolved for defining the hemodynamic significance of coronary lesions by using either static[13,14] or dynamic[9] CT imaging platforms.[6,826,28] The authors of a recent review of the benefits and shortcomings of myocardial CT perfusion techniques suggested that 1) the optimal method for assessing functional significance of coronary lesions by CT imaging remains to be established and that 2) "imperfect gold-standard comparators" should be replaced with "more valid reference standards."[5] In the present study, we investigated the limitations of a CT perfusion index used in clinical application software.

TPR during stress imaging was introduced a decade ago to improve the diagnostic accuracy of CT angiography for identifying hemodynamically significant lesions.[13] TPR takes advantage of the greater susceptibility of the endocardium to become ischemic relative to the epicardium with flow-limiting lesions.[9] Although an incremental benefit of CTP–TPR in conjunction with CT angiography has been reported in patient populations with a wide spectrum coronary lesion severities,[10-12,22] this benefit is reportedly less than that of visual assessment of perfusion defects by skilled CT examiners.[7,22,23]

In the present study, we sought to better define the accuracy with which CTP–TPR identifies segmental perfusion defects in a model specifically design to assess 'intermediate' coronary lesions. We used microsphere-based measures of endocardial and epicardial blood flow and postmortem anatomic validation of segmental perfusion areas as the standard for evaluating the accuracy of CTP–TPR. By titrating coronary occlusion to a known FFR during adenosine stress, downstream segmental perfusion defects were precisely defined in our model. Our findings suggest that 1) the optimal CTP–TPR threshold for the discrimination of functionally significant intermediate lesions is lower than previously reported for intermediate-risk populations, 2) the discrimination value for detecting segmental ischemia with intermediate lesions by CTP–TPR alone is poor (AUC = 0.581), and 3) there is poor agreement between CTP–TPR defects and visibly apparent perfusion and wall-motion defects.

The significance of our findings is best assessed in light of the history behind acceptance of this index for use with

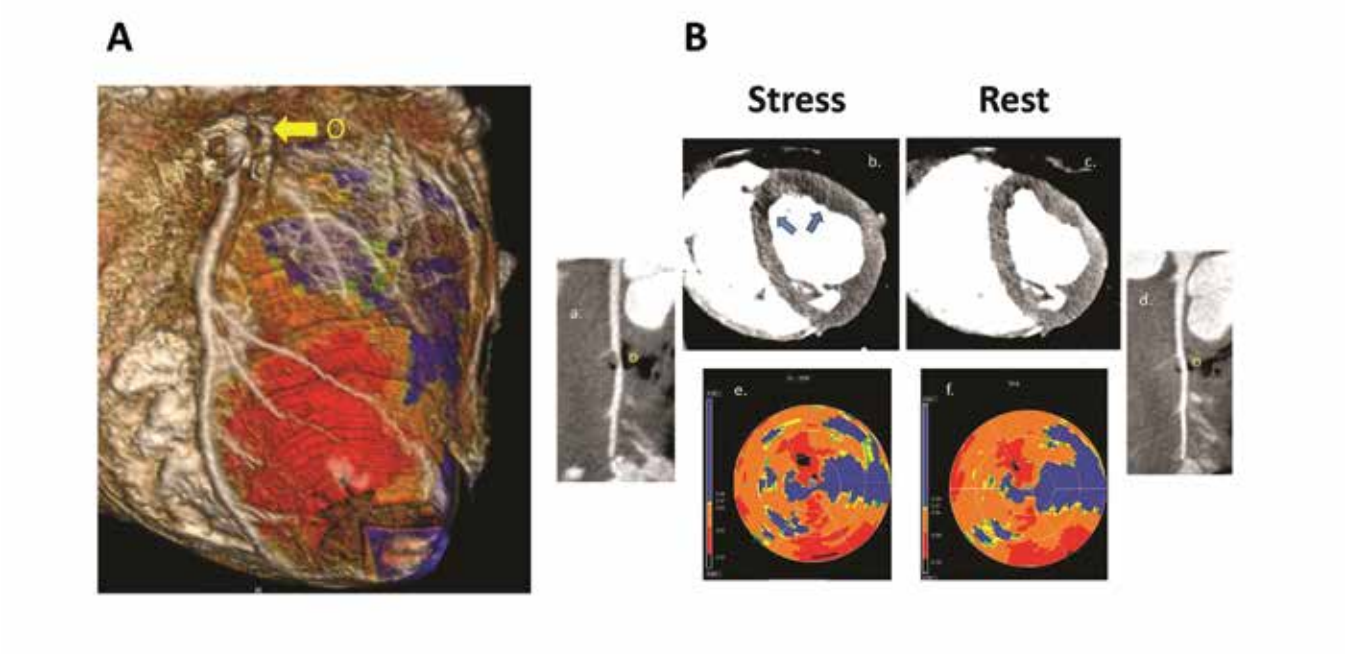

Figure 2. (A) 3D reconstructed CCTA with stress color CTP overlay. 'O' marks the location of the occluder on the LAD. (B) Stress CCTA of the LAD with 61% stenosis (a), short-axis stress CTP image at the mid-cavity level with ischemia (arrows) in the anterior and anterior septal segments of the LAD distribution (b), short-axis rest CTP image at the same level, with mild rest perfusion defect (c), rest CCTA of LAD with no perceptible stenosis (d), color polar map of the stress CTP–TPR, demonstrating multiple areas with perfusion defects in the LAD distribution (e), and color polar map of the rest CTP–TPR, demonstrating moderate defect in the LAD distribution (f).

Table 1. Segmental myocardial blood flows and TPR ratios

	Adenosine			Rest		
Myocardial blood flow (mL/min/g)	Epicardial	Endocardial	*P*[a]	Epicardial	Endocardial	*P*[a]
LAD (*n* = 60)	2.32 ± 1.19	1.99 ± 1.57	<0.004	1.69 ± 0.83	1.75 ± 0.57	0.462
Other (*n* = 100)	2.68 ± 1.40	2.23 ± 1.71	<0.001	1.72 ± 0.77	1.77 ± 0.64	0.269
LAD compared with other[b]	0.081	0.372		0.857	0.794	

	μ TPR			CTP–TPR		
TPR ratio	Stress	Rest	*P*[c]	Stress	Rest	*P*[c]
LAD (*n* = 60)	0.83 ± 0.30	1.12 ± 0.26	<0.001	0.78 ± 0.16	0.78 ± 0.13	0.871
Other (*n* = 100)	0.83 ± 0.32	1.10 ± 0.25	<0.001	0.86 ± 0.15	0.89 ± 0.13	0.138
LAD compared with other[b]	0.963	0.681		0.002	<0.001	

[a]*P* values indicate comparison of epicardial and endocardial blood flows
[b]*P* values indicate comparison of left anterior descending artery (LAD) with left circumflex and right coronary arteries (other)
[c]*P* values indicate comparison between stress and rest TPR ratios

FDA-approved coronary artery analysis software. CTP–TPR was introduced as a semiquantitative index for identifying myocardial perfusion defects in patients (*n* = 44) with a suspicion of CAD and abnormal stress SPECT images.[13] In that study, the TPR of normal segments was 1.12 ± 0.13, and perfusion defects were defined as TPR that were 1 SD below the mean (TPR less than 0.99). With this cutoff, the per-vessel or -territory sensitivity, specificity, and positive and negative predictive values were 75%, 87%, 60%, and 93%, respectively. Although SPECT myocardial perfusion imaging does not provide sufficient resolution for quantifying endocardial and epicardial perfusion, the TPR threshold of less than 0.99 was incorporated into semiautomated automated software for clinical use and in polar map displays of segmental perfusion defects. Lower optimal threshold for CTP–TPR have been reported for populations with more severe coronary stenosis.[14] Other investigators also have reported a lower TPR threshold (<0.85) with a 2-layer attenuation model for the detection of lesions that were positive by SPECT and with 70% or greater stenosis by quantitative invasive coronary angiography.[10] Furthermore, 2 groups[22,31] failed to find an incremental benefit of CTP–TPR over visual assessments of perfusion defects in patients with coronary stenosis with direct measures of FFR of 0.80 or less. These observations are consistent with our findings showing that the optimal cutoff for CTP–TPR for intermediate lesions was 0.80, with poor discriminatory value of our receiver operating characteristic analysis. The overall accuracy of CTP–TPR for identifying segmental perfusion defects with intermediate lesions in our model was 63.3%. we also found poor agreement between CTP–TPR and the visual assessment of both perfusion defects and wall-motion abnormalities.

With regard to study limitations, we used a swine model to validate the accuracy of CTP–TPR that was derived from

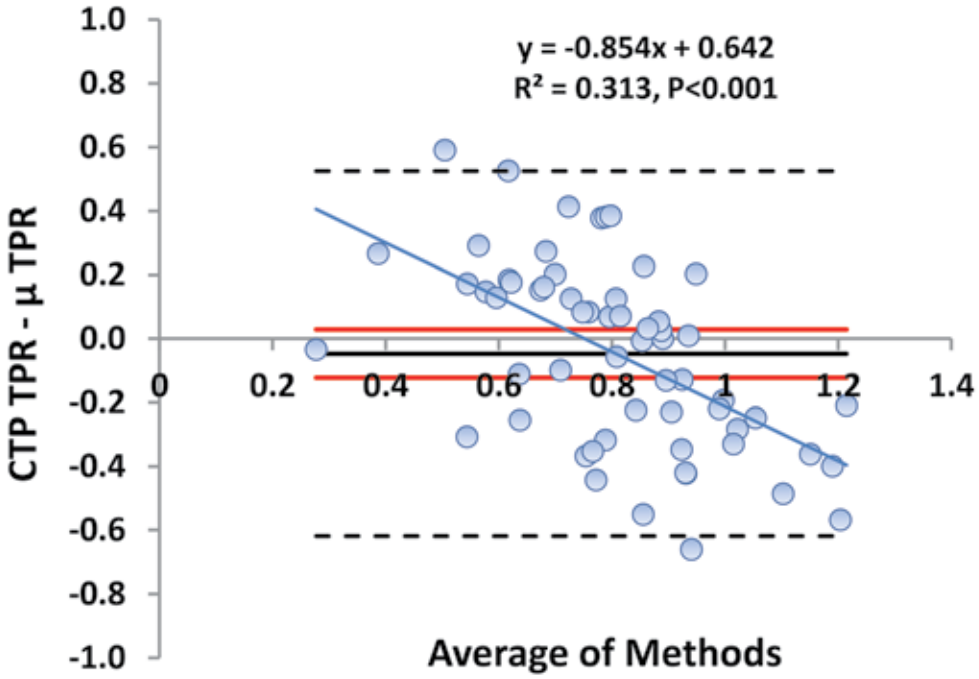

Figure 3. Bland–Altman test of agreement, illustrating poor agreement between CTP–TPR and mTPR over the mean measurement range (Δ mean ± 95% CI = –0.047 ± 0.292). The dashed lines depict the limits of agreement, and the solid red lines are the 95% CI for offset bias. The blue line illustrates the differences regressed to the mean, indicating a proportional error within the data range.

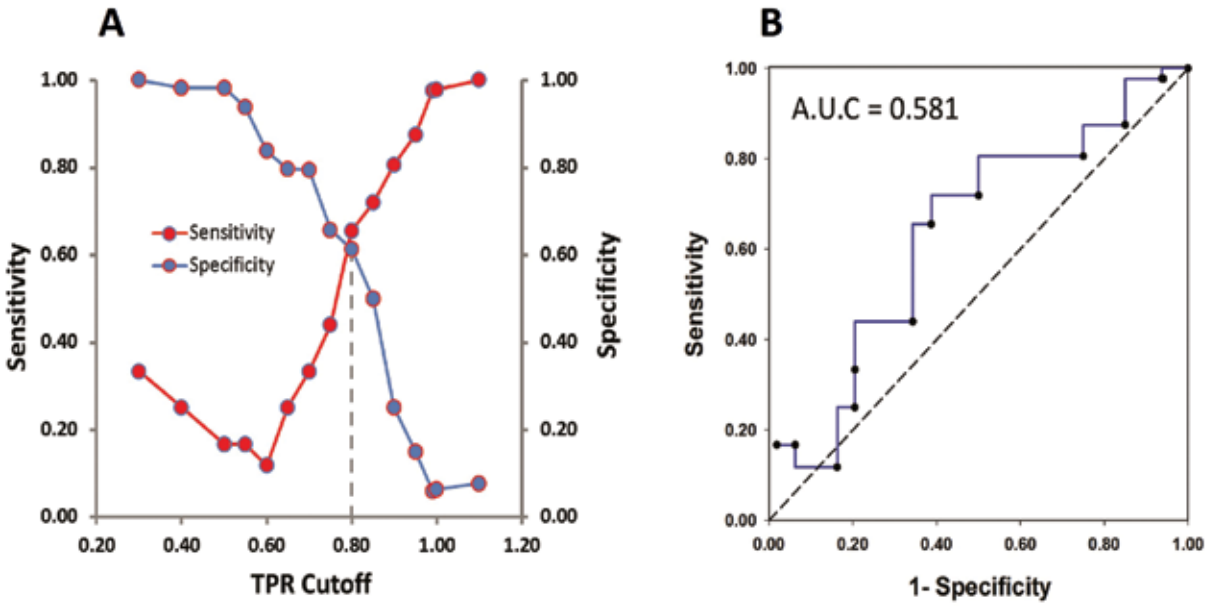

Figure 4. (A) Comparison of the sensitivity and specificity of CTP–TPR threshold values for detecting segmental perfusion defects associated with intermediate LAD lesions. The best compromise between sensitivity (65.5%) and specificity (61.3%) was at a CTP–TPR threshold of 0.80 (dashed veridical line). (B) receiver operating characteristic curve, indicating that CTP–TPR has a low discriminatory value (AUC= 0.581) for detecting perfusion defects.

software optimized for humans. Although the coronary anatomy and myocardial blood flow in swine have been well studied, the effects of partial volume, beam hardening, and motion artifacts in this model are less well defined. In the present study, perfusion segments were precisely defined by postmortem anatomy and the course of the LAD. Short-axis slices 1) began at the level of the LAD occluder, with the basal segment excluded, and 2) CT perfusion territories where matched with 1-cm–thick postmortem anatomic slices of the heart (excluding the apex) prior to CTP–TPR analysis. The TPR software that we used in this study automatically divides the myocardial wall into 3 equal layers;[13] however, our microsphere analysis was based on division of the myocardial wall into 2 layers. In addition, in our study, 4 to 5 min of transport time was required from the surgical area to the CT imaging suite. During this period, although no adjustment was made to the occluder, adenosine infusion was terminated for transport and then reestablished to maintain stable hemodynamics for 5 min after the animal was positioned

Table 2. Sensitivity, specificity, and predictive values for TPR thresholds

TPR threshold	Sensitivity	Specificity	PPV	NPV	Accuracy
0.99	97.7%	5.9%	72.4%	50.0%	71.7%
0.85	71.9%	50.0%	62.2%	60.9%	61.7%
0.80	65.5%	61.3%	61.3%	65.5%	63.3%
0.75	44.0%	65.7%	47.8%	62.2%	56.7%
0.60	11.8%	83.7%	22.2%	70.6%	63.3%

NPV, negative predictive value; PPV, positive predictive value

in the CT prior to image acquisition for stress. Finally, we opted for a stress–rest protocol design for this analysis. This approach has both advantages and limitations,[5] most notably providing the ability to perform stress imaging without pretreatment with β blockers (which can mask perfusion defects when present) but without the advantage of defining the coronary anatomy prior to administering adenosine. This protocol decision may affect the generalizability of our results but is considered a viable approach to CTP imaging.[5,6]

In conclusion, we are the first to report the use of newly introduced disposable 2-French micromanometric catheters and a standard clinical inflator with an occlusion device to establish stable experimental intermediate coronary artery lesions. We provide a method for uniform slicing of cardiac tissue to achieve anatomic correlates with cardiac CT imaging. Finally, our study shows that when corrected for chance events, only modest agreement was noted between segmental perfusion defects detected by semiautomated CT measures of TPR compared with microsphere measures of myocardial blood flow. These findings suggest that further refinements of semiautomated TPR software are warranted to improve accuracy in detecting perfusion defects in patients with intermediate lesions and also demonstrate the utility of translational models that afford the opportunity to use 'gold standard' measures of myocardial blood flow for validation.

Acknowledgments

This project was made possible by funding from the US Air Force 59th Medical Wing in collaboration with the US Army Institute of Surgical Research (USA ISR), Joint Base San Antonio, TX.

The view(s) expressed herein are those of the authors and do not reflect the official policy or position of Brooke Army Medical Center, the US Army Medical Department, the US Army Office of the Surgeon General, the Department of the Army, the Department of the Air Force, the Department of Defense, or the US Government.

The animal protocol was reviewed and approved by the IACUC at the US Army Institute of Surgical Research (protocol no. A-2017-01). This study has been conducted in compliance with the Animal Welfare Act, implementing Animal Welfare Regulations, and the principles of the *Guide for the Care and Use of Laboratory Animals*.

References

1. **Bamberg F, Marcus RP, Becker A, Hildebrandt K, Bauner K, Schwarz F, Greif M, von Ziegler F, Bischoff B, Becker HC, Johnson TR, Reiser MF, Nikolaou K, Theisen D.** 2014. Dynamic myocardial CT perfusion imaging for evaluation of myocardial ischemia as determined by MR imaging. JACC Cardiovasc Imaging **7:**267–277. https://doi.org/10.1016/j.jcmg.2013.06.008.
2. **Bittencourt MS, Hulten EA, Murthy VL, Cheezum M, Rochitte CE, Di Carli MF, Blankstein R.** 2016. Clinical outcomes after evaluation of stable chest pain by coronary computed tomographic angiography versus usual care. Circ Cardiovasc Imaging **9:**e004419. https://doi.org/10.1161/CIRCIMAGING.115.004419.
3. **Blankstein R, Shturman LD, Rogers IS, Rocha-Filho JA, Okada DR, Sarwar A, Soni AV, Bezerra H, Ghoshhajra BB, Petranovic M, Loureiro R, Feuchtner G, Gewirtz H, Hoffmann U, Mamuya WS, Brady TJ, Cury RC.** 2009. Adenosine-induced stress myocardial perfusion imaging using dual-source cardiac computed tomography. J Am Coll Cardiol **54:**1072–1084. https://doi.org/10.1016/j.jacc.2009.06.014.
4. **Blankstein R, Di Carli MF.** 2010. Integration of coronary anatomy and myocardial perfusion imaging. Nat Rev Cardiol **7:**226–236. https://doi.org/10.1038/nrcardio.2010.15.
5. **Branch KR, Haley RD, Bittencourt MS, Patel AR, Hulten E, Blankstein R.** 2017. Myocardial computed tomography perfusion. Cardiovasc Diagn Ther **7:**452–462. https://doi.org/10.21037/cdt.2017.06.11.
6. **Bucher AM, De Cecco CN, Schoepf UJ, Wang R, Meinel FG, Binukrishnan SR, Spearman JV, Vogl TJ, Ruzsics B.** 2014. Cardiac CT for myocardial ischaemia detection and characterization—comparative analysis. Br J Radiol **87:**20140159. https://doi.org/10.1259/bjr.20140159.
7. **Cademartiri F, Seitun S, Clemente A, La Grutta L, Toia P, Runza G, Midiri M, Maffei E.** 2017. Myocardial blood flow quantification for evaluation of coronary artery disease by computed tomography. Cardiovasc Diagn Ther **7:**129–150. https://doi.org/10.21037/cdt.2017.03.22.
8. **Chen J, Pu Y, Zhang Z, Yu X, Yang Z.** 2017. Detection of hemodynamically significant coronary artery stenosis with CT enhancement ratio: a validation study in a porcine model. AJR Am J Roentgenol **209:**103–109. https://doi.org/10.2214/AJR.16.16698.
9. **Coenen A, Lubbers MM, Kurata A, Kono A, Dedic A, Chelu RG, Dijkshoorn ML, Rossi A, van Geuns RM, Nieman K.** 2016. Diagnostic value of transmural perfusion ratio derived from dynamic CT-based myocardial perfusion imaging for the detection of haemodynamically relevant coronary artery stenosis. Eur Radiol **27:**2309–2316. https://doi.org/10.1007/s00330-016-4567-0.
10. **Cury RC, Magalhães TA, Paladino AT, Shiozaki AA, Perini M, Senra T, Lemos PA, Cury RC, Rochitte CE.** 2011. Dipyridamole stress and rest transmural myocardial perfusion ratio evaluation by 64 detector-row computed tomography. J Cardiovasc Comput Tomogr **5:**443–448. https://doi.org/10.1016/j.jcct.2011.10.012.
11. **Feuchtner G, Goetti R, Plass A, Wieser M, Scheffel H, Wyss C, Stolzmann P, Donati O, Schnabl J, Falk V, Alkadhi H, Leschka S, Cury RC.** 2011. Adenosine stress high-pitch 128-slice dual-source myocardial computed tomography perfusion for imaging of reversible myocardial ischemia: comparison with magnetic resonance imaging. Circ Cardiovasc Imaging **4:**540–549. https://doi.org/10.1161/CIRCIMAGING.110.961250.
12. **Fihn SD, Blankenship JC, Alexander KP, Bittl JA, Byrne JG, Fletcher BJ, Fonarow GC, Lange RA, Levine GN, Maddox TM, Naidu SS, Ohman EM, Smith PK.** 2014. 2014 ACC/AHA/AATS/PCNA/SCAI/STS focused update of the guideline for the diagnosis and management of patients with stable ischemic heart disease: a report of the American College of Cardiology/American Heart Association Task Force on Practice Guidelines, and the American Association for Thoracic Surgery, Preventive Cardiovascular Nurses Association, Society for Cardiovascular Angiography and Interventions, and Society of Thoracic Surgeons. J Am Coll Cardiol **64:**1929–1949. https://doi.org/10.1016/j.jacc.2014.07.017.
13. **George RT, Arbab-Zadeh A, Miller JM, Kitagawa K, Chang HJ, Bluemke DA, Becker L, Yousuf O, Texter J, Lardo AC, Lima JA.** 2009. Adenosine stress 64- and 256-row detector computed tomography angiography and perfusion imaging: a pilot study evaluating the transmural extent of perfusion abnormalities to

predict atherosclerosis causing myocardial ischemia. Circ Cardiovasc Imaging **2:**174–182. https://doi.org/10.1161/CIRCIMAGING.108.813766.

14. **George RT, Arbab-Zadeh A, Miller JM, Vavere AL, Bengel FM, Lardo AC, Lima JA.** 2012. Computed tomography myocardial perfusion imaging with 320-row detector computed tomography accurately detects myocardial ischemia in patients with obstructive coronary artery disease. Circ Cardiovasc Imaging **5:**333–340. https://doi.org/10.1161/CIRCIMAGING.111.969303.
15. **George RT, Mehra VC, Chen MY, Kitagawa K, Arbab-Zadeh A, Miller JM, Matheson MB, Vavere AL, Kofoed KF, Rochitte CE, Dewey M, Yaw TS, Niinuma H, Brenner W, Cox C, Clouse ME, Lima JA, Di Carli M.** 2014. Myocardial CT perfusion imaging and SPECT for the diagnosis of coronary artery disease: a head-to-head comparison from the CORE320 multicenter diagnostic performance study. Radiology **272:**407–416. https://doi.org/10.1148/radiol.14140806.
16. **Goldstein JA, Chinnaiyan KM, Abidov A, Achenbach S, Berman DS, Hayes SW, Hoffmann U, Lesser JR, Mikati IA, O'Neil BJ, Shaw LJ, Shen MY, Valeti US, Raff GL; CT-STAT Investigators.** 2011. The CT-STAT (Coronary computed tomographic angiography for systematic triage of acute chest pain patients to treatment) trial. J Am Coll Cardiol **58:**1414–1422. https://doi.org/10.1016/j.jacc.2011.03.068.
17. **Gonzalez JA, Lipinski MJ, Flors L, Shaw PW, Kramer CM, Salerno M.** 2015. Meta-analysis of diagnostic performance of coronary computed tomography angiography, computed tomography perfusion, and computed tomography-fractional flow reserve in functional myocardial ischemia assessment versus invasive fractional flow reserve. Am J Cardiol **116:**1469–1478. https://doi.org/10.1016/j.amjcard.2015.07.078.
18. **Hoffmann U, Truong QA, Schoenfeld DA, Chou ET, Woodard PK, Nagurney JT, Pope JH, Hauser TH, White CS, Weiner SG, Kalanjian S, Mullins ME, Mikati I, Peacock WF, Zakroysky P, Hayden D, Goehler A, Lee H, Gazelle GS, Wiviott SD, Fleg JL, Udelson JE; ROMICAT-II Investigators.** 2012. Coronary CT angiography versus standard evaluation in acute chest pain. N Engl J Med **367:**299–308. https://doi.org/10.1056/NEJMoa1201161.
19. **Hulten E, Ahmadi A, Blankstein R.** 2015. CT assessment of myocardial perfusion and fractional flow reserve. Prog Cardiovasc Dis **57:**623–631. https://doi.org/10.1016/j.pcad.2015.03.003.
20. **Institute for Laboratory Animal Research.** 2011. Guide for the care and use of laboratory animals, 8th ed. Washington (DC): National Academies Press.
21. **Jones RL, Thomas DM, Barnwell ML, Fentanes E, Young AN, Barnwell R, Foley AT, Hilliard M, Hulten EA, Villines TC, Cury RC, Slim AM.** 2014. Safe and rapid disposition of low-to-intermediate risk patients presenting to the emergency department with chest pain: a 1-year high-volume single-center experience. J Cardiovasc Comput Tomogr **8:**375–383. https://doi.org/10.1016/j.jcct.2014.08.003.
22. **Ko BS, Cameron JD, Leung M, Meredith IT, Leong DP, Antonis PR, Crossett M, Troupis J, Harper R, Malaiapan Y, Seneviratne SK.** 2012. Combined CT coronary angiography and stress myocardial perfusion imaging for hemodynamically significant stenoses in patients with suspected coronary artery disease: a comparison with fractional flow reserve. JACC Cardiovasc Imaging **5:**1097–1111. https://doi.org/10.1016/j.jcmg.2012.09.004.
23. **Magalhães TA, Kishi S, George RT, Arbab-Zadeh A, Vavere AL, Cox C, Matheson MB, Miller JM, Brinker J, Di Carli M, Rybicki FJ, Rochitte CE, Clouse ME, Lima JA.** 2015. Combined coronary angiography and myocardial perfusion by computed tomography in the identification of flow-limiting stenosis - The CORE320 study: an integrated analysis of CT coronary angiography and myocardial perfusion. J Cardiovasc Comput Tomogr **9:**438–445. https://doi.org/10.1016/j.jcct.2015.03.004.
24. **Mark DB, Berman DS, Budoff MJ, Carr JJ, Gerber TC, Hecht HS, Hlatky MA, Hodgson JM, Lauer MS, Miller JM, Morin RL, Mukherjee D, Poon M, Rubin GD, Schwartz RS.** 2010. ACCF/ACR/AHA/NASCI/SAIP/SCAI/SCCT 2010 expert consensus document on coronary computed tomographic angiography: A report of the American College of Cardiology Foundation Task Force on Expert Consensus Documents. J Am Coll Cardiol **55:**2663–2699. https://doi.org/10.1016/j.jacc.2009.11.013.
25. **Moss AJ, Williams MC, Newby DE, Nicol ED.** 2017. The Updated NICE Guidelines: Cardiac CT as the first-line test for coronary artery disease. Curr Cardiovasc Imaging Rep **10:**1–7. https://doi.org/10.1007/s12410-017-9412-6.
26. **Ramsey BC, Fentanes E, Choi AD, Branch KR, Thomas DM.** 2018. Myocardial assessment with Cardiac CT: ischemic heart disease and beyond. Curr Cardiovasc Imaging Rep 11**:1–**16. https://doi.org/10.1007/s12410-018-9456-2. PubMed
27. **Reinhardt CP, Dalhberg S, Tries MA, Marcel R, Leppo JA.** 2001. Stable labeled microspheres to measure perfusion: validation of a neutron activation assay technique. Am J Physiol Heart Circ Physiol **280:**H108–H116. https://doi.org/10.1152/ajpheart.2001.280.1.H108.
28. **Rossi A, Merkus D, Klotz E, Mollet N, de Feyter PJ, Krestin GP.** 2014. Stress myocardial perfusion: imaging with multidetector CT. Radiology **270:**25–46. https://doi.org/10.1148/radiol.13112739.
29. **Sørgaard MH, Kofoed KF, Linde JJ, George RT, Rochitte CE, Feuchtner G, Lima JA, Abdulla J.** 2016. Diagnostic accuracy of static CT perfusion for the detection of myocardial ischemia. A systematic review and meta-analysis. J Cardiovasc Comput Tomogr **10:**450–457. https://doi.org/10.1016/j.jcct.2016.09.003.
30. **US Department of Agriculture.** 2017. USDA Animal Care: Animal Welfare Act and Animal Welfare Regulations. United States Department of Agriculture. [Cited 04 April 2020]. Available at: https://www.aphis.usda.gov/aphis/ourfocus/animalwelfare/sa_awa
31. **Yang DH, Kim YH, Roh JH, Kang JW, Han D, Jung J, Kim N, Lee JB, Ahn JM, Lee JY, Park DW, Kang SJ, Lee SW, Lee CW, Park SW, Park SJ, Lim TH.** 2015. Stress myocardial perfusion CT in patients suspected of having coronary artery disease: visual and quantitative analysis—validation by using fractional flow reserve. Radiology **276:**715–723. https://doi.org/10.1148/radiol.2015141126.